Optical Fiber Technology 69 (2022) 102843

Contents lists available at ScienceDirect

Optical Fiber Technology

journal homepage: www.elsevier.com/locate/yofte

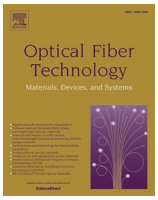

Dual tapered optical fiber for simultaneous detection of curvature and strain

J.R. Ek-Ek [a,b], D. Jauregui-Vazquez [a,c], J.P. Korterik [a], M. Benedictus [a], F. Martinez-Pinon [b], H. L. Offerhaus [a], J.A. Alvarez-Chavez [a,*]

[a] Optical Sciences Group - University of Twente, Drienerlolaan 5, 7522 NB Enschede, The Netherlands
[b] Instituto Politecnico Nacional, Centro de Investigacion e Innovacion Tecnologica, Alcaldía Azcapotzalco, CP 02250 Ciudad de Mexico, Mexico
[c] Departamento de Ingeniería Electrónica, División de Ingenierías Campus Irapuato Salamanca, Universidad de Guanajuato, Carretera Salamanca-Valle de Santiago km 3.5 + 1.8 km, Salamanca, Gto. 36885, Mexico

ARTICLE INFO

Keywords:
Fiber
Sensor
Curvature
Strain
Taper

ABSTRACT

We present a study of simultaneous detection of curvature and strain in optical fiber. This contains a micro tapered section and a nano tapered section. The transmission spectrum shows interference of multiple modes, and the frequency of the modulation can be used to distinguish and monitor specific physical parts of the fiber structure. The curvature detection is achieved using one specific modulation frequency component; this component shows an intensity modulation with a sensitivity of 0.26 dB/m^{-1}. The strain information is extracted by applying a phase analysis over a second spatial frequency component; this analysis shows a sensitivity close to 8 mrad/με. The strain phase analysis exhibits a linear response, and the intensity curvature data indicates an exponential model. The proposed signal analysis can be employed for simultaneous detection in optical fiber interferometric sensors.

1. Introduction

For more than four decades, optical fiber tapers have been explored for a wide variety of applications such as nonlinear effects [1,2], selective optical fiber filters [3,4], optical fiber sensors [5,6], biosensing purposes [7], optical trapping and molecular manipulation [8,9], fiber optics lasers [10,11] and plasmonic devices [12,13]. Furthermore, the interferometric response of the optical fiber tapers have been used to monitoring refractive index [14,15], curvature [16,17], strain [18], angle [19–21], magnetic field [19,22], pressure [23,24], and many others parameters as well simultaneous combinations of parameters. The wide reach of sensing applications stem from the advantageous characteristics: high sensitivity, straightforward fabrication, possibilities for mass production, and cost-effective demodulation setups. As can be appreciated, the optical fiber taper profile offers numerous advantages. Consequently, many efforts have been made to achieve an optimized tapered profile in Single-Mode Fibers (SMF) and Multimode Fibers (MMF) [25,26]. Furthermore, by using a mono-molecular coated taper profile, the detection of biomolecules is possible [26,27].

At the same time the simultaneous detection of multiple parameters is under current investigation. One approach based on tapered fibers focused on detecting refractive index and temperature [28]. Phase modulation direction was used to detect both parameters simultaneously; however, phase modulation was also presented for most of other parameters. Another approach for simultaneous detection uses a Fiber Bragg Grating (FBG) [29]; This structure can also be tapered for parameter discrimination [25,26]. One parameter can be detected through changes in the FBG and the second parameter by monitoring the interferometric effects related to the taper. Fully independent measurement is not achieved; both structures are also sensitive to other parameters, and some crosstalk in the phase modulation is present for the parameters of interest. Switching to amplitude modulation presents challenges related to power fluctuations. Similarly, configurations that rely on the detection of wavelength-shifts also suffer from ambiguity and crosstalk for simultaneous detection. In this work, simultaneous detection of curvature and strain is proposed and demonstrated using the modulation frequency spectrum. The curvature is detected at one modulation frequency where the intensity shows a linear variation; Meanwhile, the strain is detected by extracting the phase of another modulation frequency component. As a result, both parameters can be

* Corresponding author.
E-mail address: j.a.alvarezchavez@utwente.nl (J.A. Alvarez-Chavez).

https://doi.org/10.1016/j.yofte.2022.102843
Received 23 November 2021; Received in revised form 3 February 2022; Accepted 6 February 2022
Available online 11 February 2022

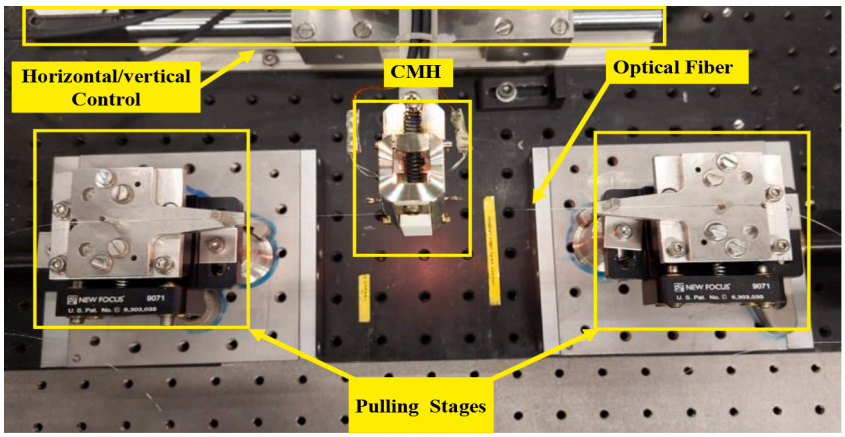

Fig. 1. Experimental fabrication setup of micro/nano optical fiber tapers: Two horizontal pulling stages and a combined horizontal/vertical stage to control the heat-source position.

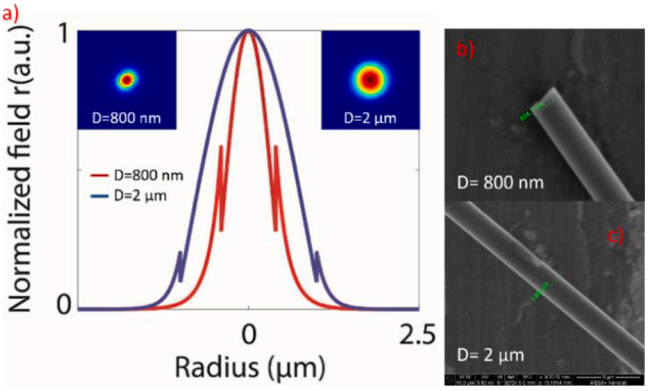

Fig. 2. a) Comparison of the mode field intensity at 1 μm wavelength with fiber diameter of 800 nm and 2 μm. Taper waist measured in the Scanning Electron Microscope of b) Taper 2 and c) Taper1.

estimated simultaneously.

2. Fabrication and model of micro/nano tapered optical fibers

The fabrication setup consists of three computer-controlled horizontal translation stages: two for pulling the optical fiber and one for moving and holding the heat source. In this work, we use a Ceramic Micro Heater (CMH-7019) controlled by a driver current as a heating element [30]. The setup diagram is shown in Fig. 1. The tapering process is controlled by a LabVIEW code, written for this purpose. A short piece of single mode fiber (SMF-28) is slowly pulled in both directions, while the CMH is moved back and forth along the fiber. In this work, we focus on SMF optical taper structures because they are more suitable for generating an evanescent wave [25].

The main parameters used to determine the shape of the optical fiber taper are the temperature (°C), the motion of the CMH (moving back and forth at a speed of 0,5 mm/s), the pre-heating time (10 s), the pulling speed (0.1 mm/s), and the total distance of pulling. The temperature needs to be above 1200 °C for the softening of the glass. Pre-heating is necessary to avoid pulling the fiber too abruptly. It is possible to fabricate micro/nano optical fiber tapers in this way.

For these experiments, we prepared a micro-taper (T1) with a waist

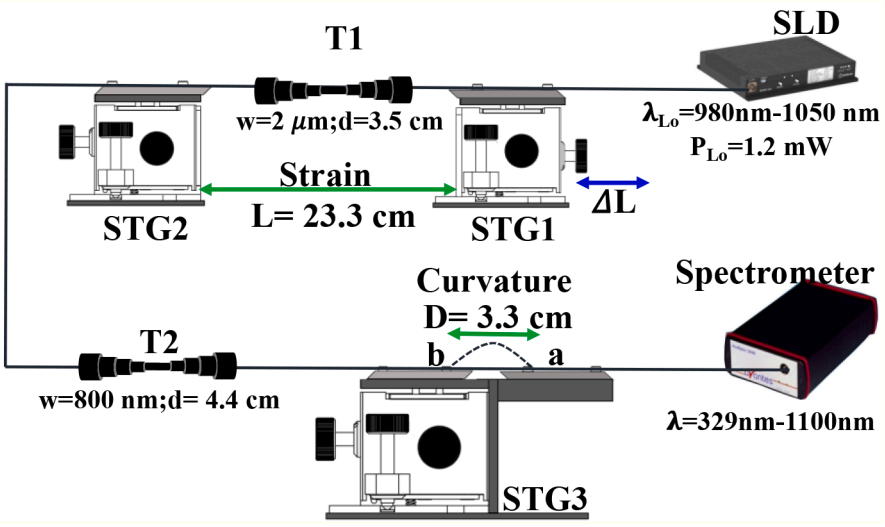

Fig. 3. Curvature-Strain sensing setup: A Super Luminescent Diode (SLD) launches the light into to the first Taper (T1), which is suspended between two translation stages (STG1 and STG2) where the strain is applied. The light then progresses 110 cm to T2. After T2, the curvature is applied on STG3. Using a fixed (a) and movable (b) point, it is possible to control the fiber bending. The signal with the curvature-strain information is detected using a spectrometer.

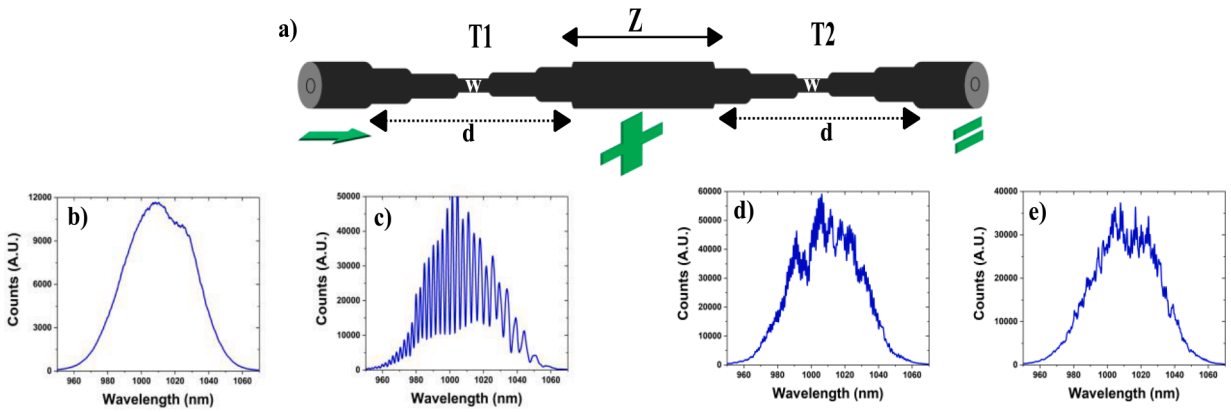

Fig. 4. a) Concatenated optical fiber structure, b) SLD spectrum, interference spectrums of c) T1, d) T2 and e) interferometric response of concatenated optical fibers tapers.

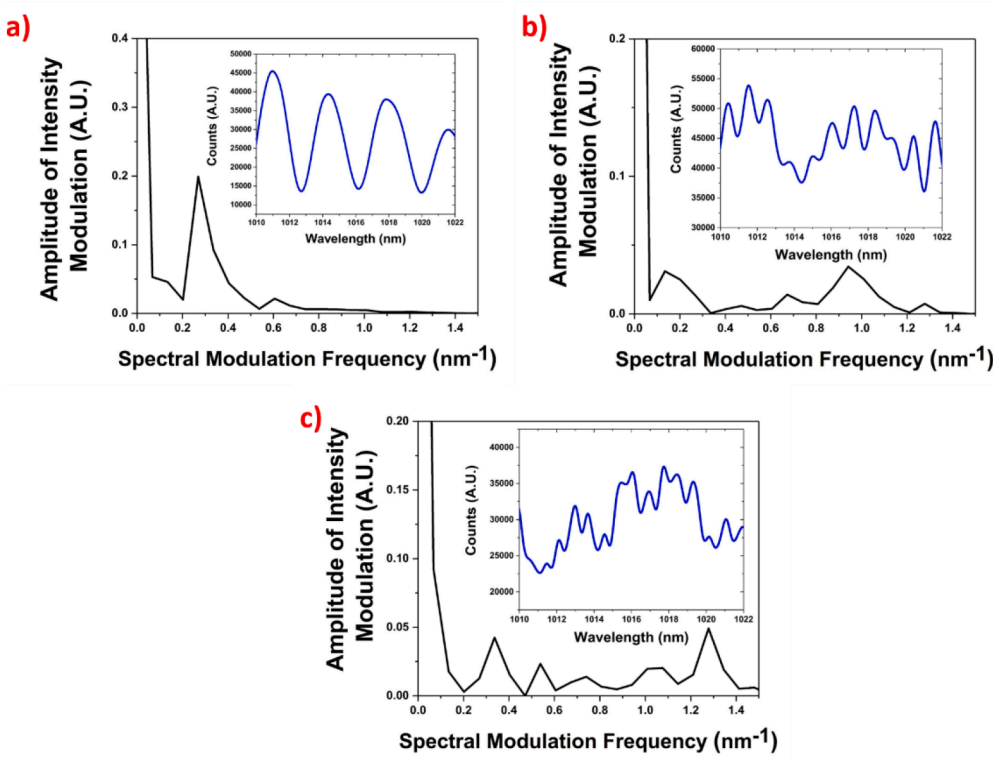

Fig. 5. Interference spectrums and its Fast Fourier Transform of a) T1, b) T2 and c) the concatenated optical fiber taper.

diameter (w) of 2 μm, (a pulling distance of 56 mm is programmed) and a nano-taper (T2) with a w = 800 nm (pulling distance of 48 mm is programmed). These dimensions were chosen while considering the minimal losses and repeatability achieved by the fabrication setup. It is important to notice that in the nano-taper (T2), the fiber diameter becomes smaller than the wavelength of the light propagating trough the optical fiber structure so that the light is no longer confined in the glass. A considerable fraction of the light propagates as an evanescent field outside the physical boundary of the fiber. Fig. 2a) shows the mode field profiles for the tapers T1 and T2 interacting with light of 1 μm wavelength. The 2D results were obtained using COMSOL. This demonstrates the presence of the evanescent field that is propagated around the fiber [31]. Fig. 2b) and c) shows the taper waist diameter of the T1 and T2 measured in the Scanning Electron Microscope (SEM).

3. Sensing setup

The transmission sensing setup includes a Super Luminescent Diode (SLD), the concatenated tapered optical fiber structure, and a spectrometer. Light from the SLD (SLD-521-HP-PM) is launched to the concatenated tapered optical fiber structure. The transmission spectrum is monitoring by the spectrometer (AvaSpec-3648). A sketch of the simultaneous detection of curvature and strain is depicted in Fig. 3.

- Strain: The strain is detected on the micro-optical fiber taper (T1); T1 was set between two X-Y-Z translation stages (STG1 and STG2). The distance between these translations stages is L = 23.3 cm (see Fig. 3). To apply the strain, the translation stage STG1 is moved in forward and backward direction (ΔL); as a result, it is possible to control the strain in a range from 128 με to 429 με.

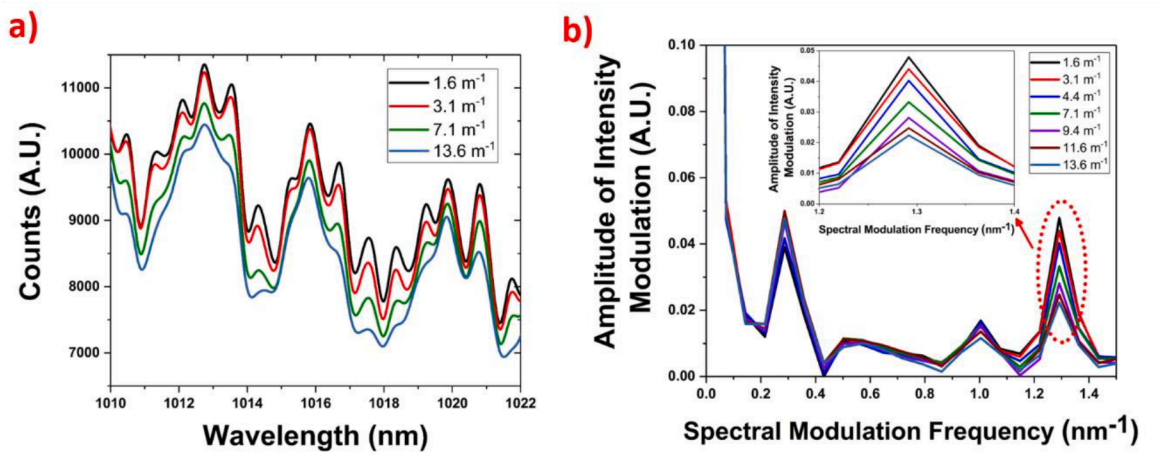

Fig. 6. First sample a) Wavelength spectral response as the curvature increases and b) its Fast Fourier transform. Inset: intensity modulation generated by specific peak component.

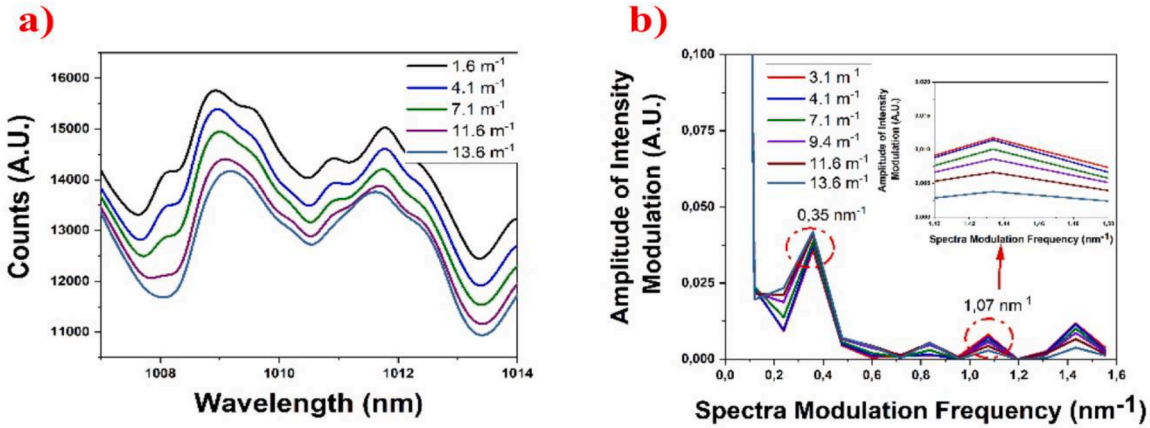

Fig. 7. Second probe a) Wavelength spectrum and b) its Fast Fourier transform response as the curvature increases. Inset: intensity modulation generated by specific peak component.

- Curvature: The curvature is applied at 25 cm from the nano-optical fiber taper T2; this distance was arbitrarily chosen (see Fig. 3). Here, the translation stage STG3 is used to control the bending radius; one point of the un-tapered optical fiber is fixed (b), and the second point (a) is moved forward and backward. The curvature varied from 1.6 m^{-1} to 13.6 m^{-1}.

4. Principle of operation

The tapered optical fiber acts as a Mach-Zehnder interferometer [24]. Here, the thin core of the tapered optical fiber provides one optical path; meanwhile, the cladding provides the second optical path, and a phase difference is generated between the path/modes. When the modes recombine at the end of the taper, an interferometric modulation of the transmission spectrum is found. This interference spectrum strongly depends on the cladding and the core modes generated by the tapered region. The interaction of these modes is governed by:

$$I_T = 2\sum_{n<m=1,N}\sqrt{I_n I_m}\cos\Delta\varnothing_{n,m}$$

where I_m and I_n represent the core and cladding modes, respectively. The phase between these modes is expressed by $\Delta\varnothing_{n,m}$; this phase difference depends on the taper length (L), the differences in the effective refractive index (Δn) and the operation wavelength (λ); The difference phase can be expressed as $\Delta\varnothing_{n,m} = 2\Delta nL/\lambda$. The relevant parts of the optical fiber structure are shown in Fig. 4.

The first taper (T1) generates an interference spectrum with a spectral modulation period of 3.4 nm (see inset Fig. 4c). This optical taper has a length of 3.5 cm and a waist diameter (w) close to 2 μm. The second taper (T2) has a waist diameter (w) of 800 nm and a length of 4.4 cm; this optical fiber taper provides the spectrum shown inset Fig. 4d); and its spectrum has two modulation periods, one of 0.92 nm and the second one 3.7 nm; This spectrum is related to the optical paths generated by the nano-tapered optical fiber. Considering the wavelength used in our experiments the nano fiber provides three optical paths: the core, cladding and surrounding media. As a result, the transmission optical spectrum shows multiple interferences.

Both spectra are combined, and the combined response is presented in the inset in Fig. 4e). A distance of 110 cm separates both optical fiber tapers. To analyze the modal contribution, the interference spectra were Fourier transformed. The interference spectrum of the first optical fiber taper is mainly composed of a core mode (DC component) and one interfering higher order mode (see Fig. 5a). The period of the modulation is related to the refractive index difference between the core and cladding mode. The second spectrum generated by T2 is composed of the core mode and two higher order modes (see Fig. 5b); The first modulation frequency is centered at 0.13 nm^{-1}, while the second frequency modulation is higher (0.94 nm^{-1}), corresponding to the small modulation period. The modes at higher modulation frequency components are mainly in the optical fiber cladding. All the generated modes combine in

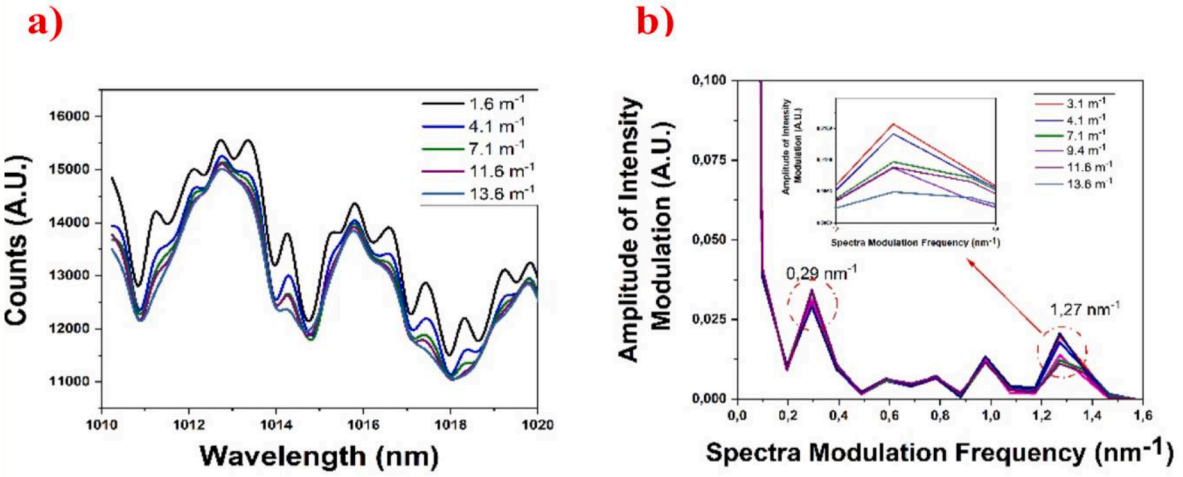

Fig. 8. a) Wavelength spectrum and b) its Fast Fourier transform response as the curvature of the probe 3 increases. Inset: intensity modulation generated by specific peak component.

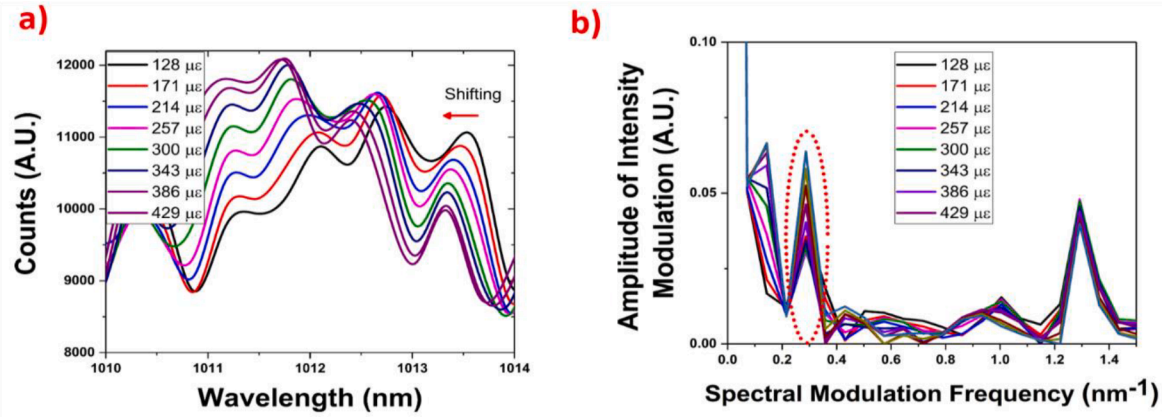

Fig. 9. a) Strain response for small increments around 43 με and b) the spatial frequency analysis of probe 1,

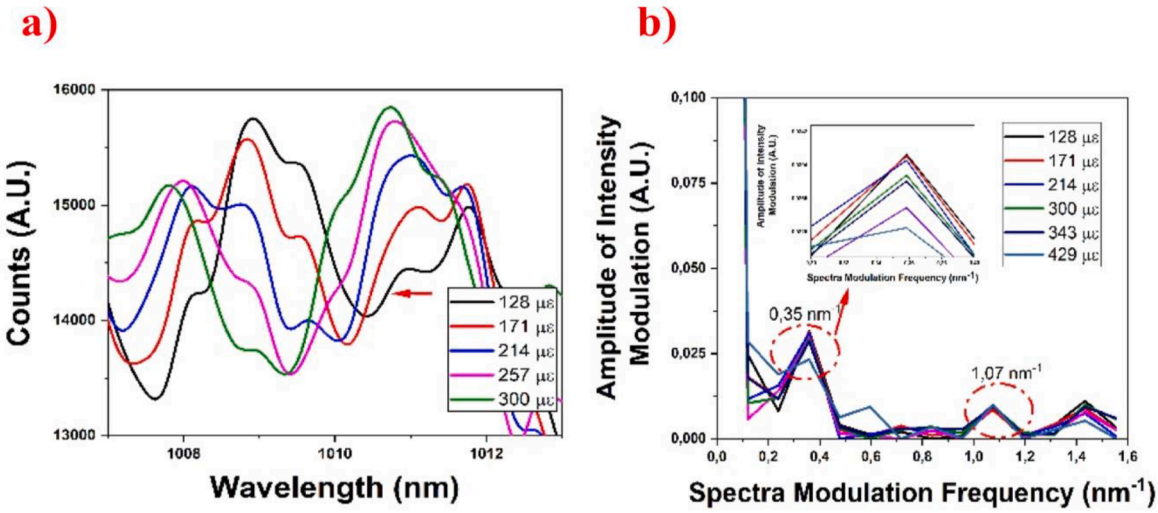

Fig. 10. Second probe a) Strain response and b) the spatial frequency analysis, inset: phase data extracted from the peak component centered at 0. 35 nm^{-1}.

the final interference spectrum, showing modulation frequencies centered at 0.33 nm^{-1} and 1.27 nm^{-1} (see Fig. 5c).

5. Results

To demonstrate simultaneous detection of curvature and strain, both parameters are analyzed using the sensing setup in Fig. 3. It is essential

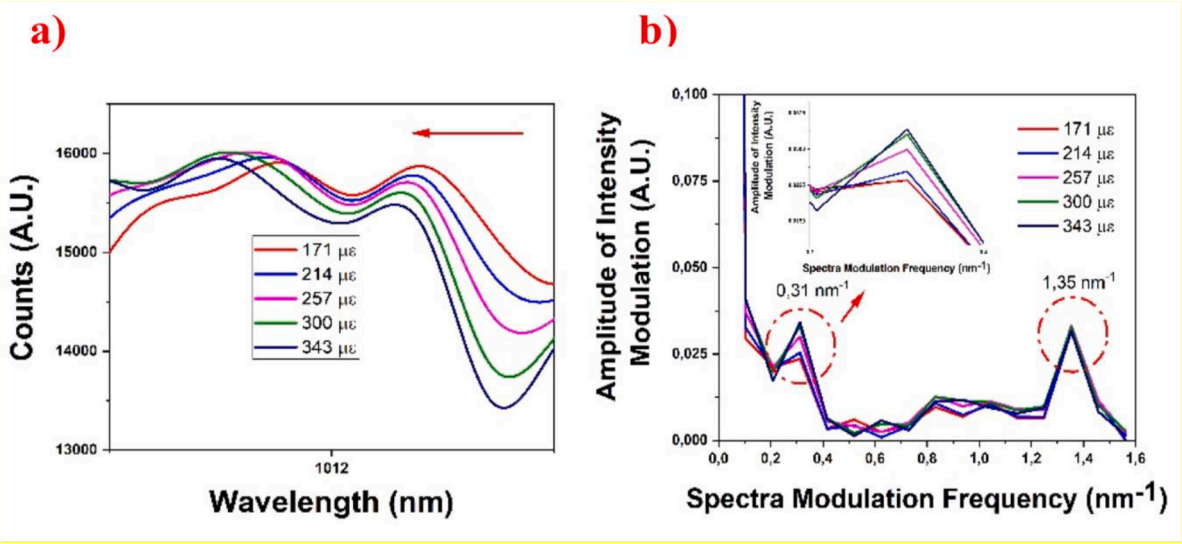

Fig. 11. a) Wavelength spectrum response as the strain increases and its b) spatial frequency spectra.

Table 1
Peak components used for strain and curvature detection.

Probe	Strain-Peak component (nm^{-1})	Curvature-Peak component (nm^{-1})
Probe 1	0.29	1.27
Probe 2	0.35	1.07
Probe 3	0.31	1.35

to note that three probes were fabricated, for which their repeatability was analyzed. The first parameter to be analyzed is curvature. It is important to note that a section of fiber without tapering is used to induce and sense the curvature, not the tapered section itself. The curvature effect over the wavelength interference spectrum of the first probe can be observed in Fig. 6a; here, a specific wavelength range is used to analyze the curvature. It can be observed that the overall intensity decreases slightly. More importantly, the high frequency modulations disappear as the curvature increases (see Fig. 6a). The Fourier

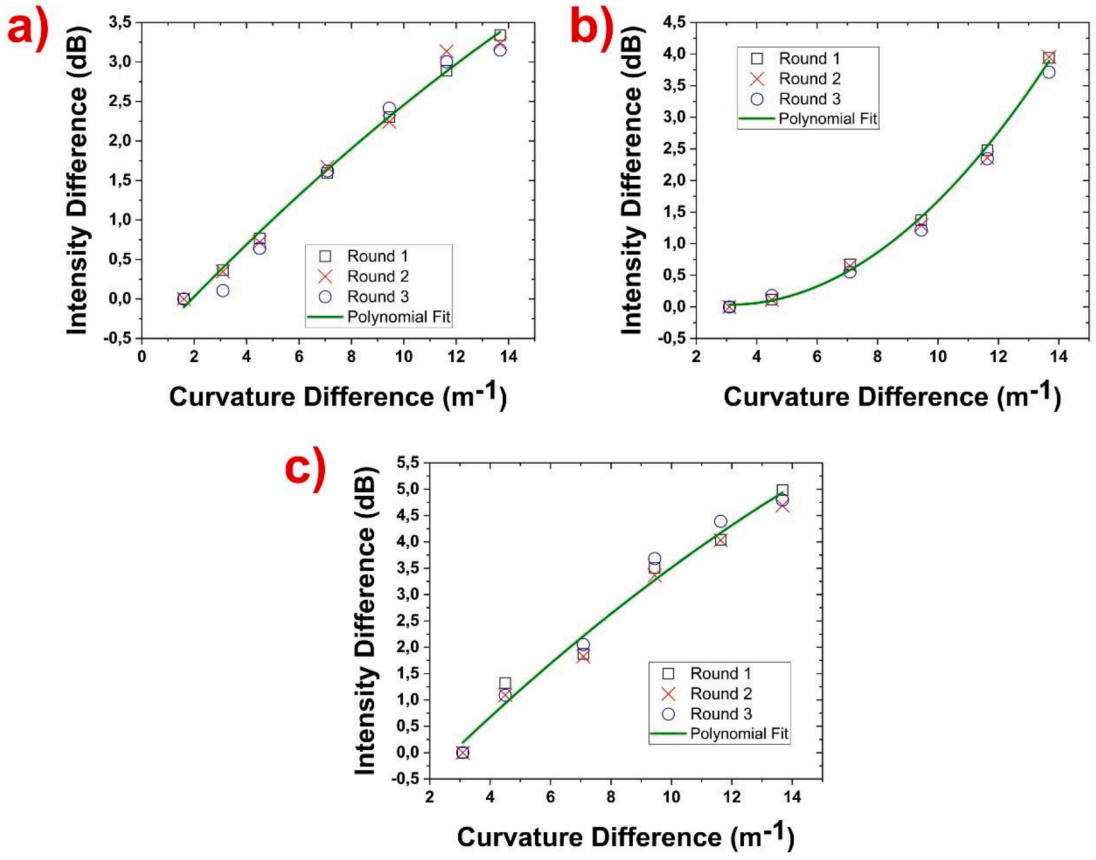

Fig. 12. Intensity analysis of the curvature peak after three consecutive rounds: a) Probe 1, b) Probe 2 and c) Probe 3.

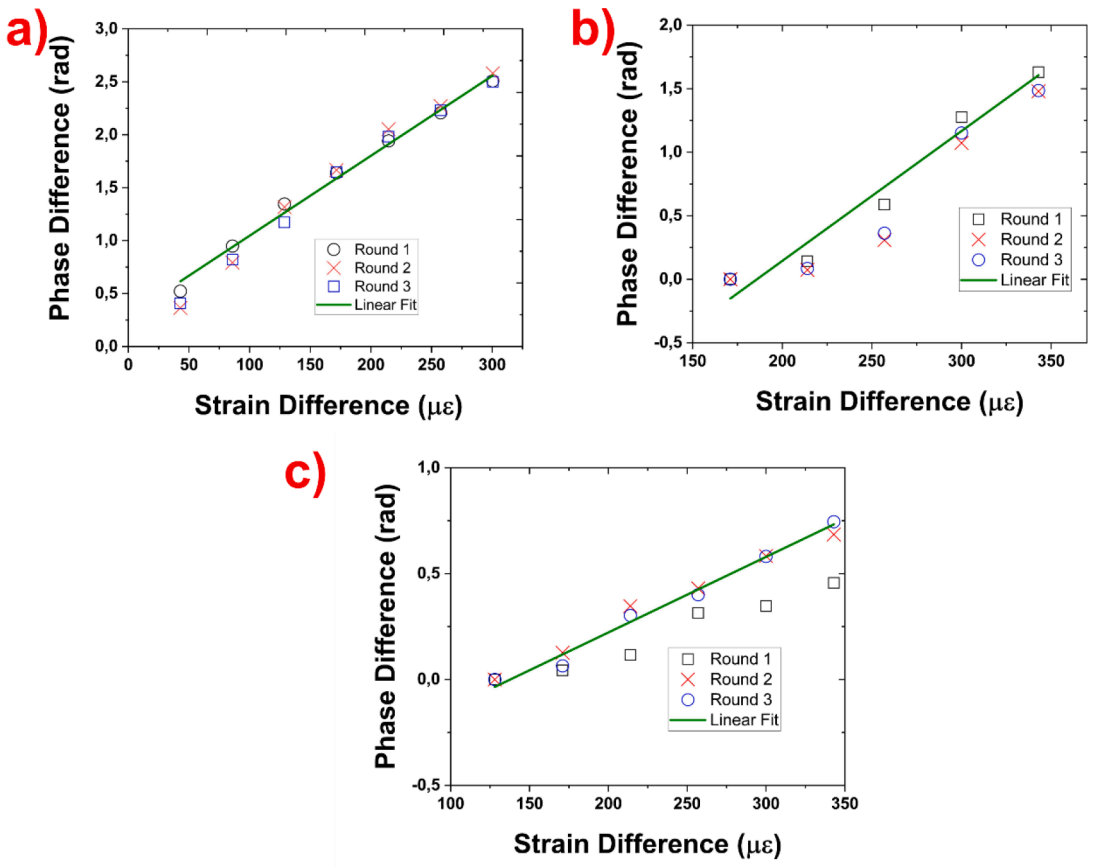

Fig. 13. Strain analysis of (a) probe 1, (b) probe 2 and (c) probe 3, after three consecutive rounds for each probe.

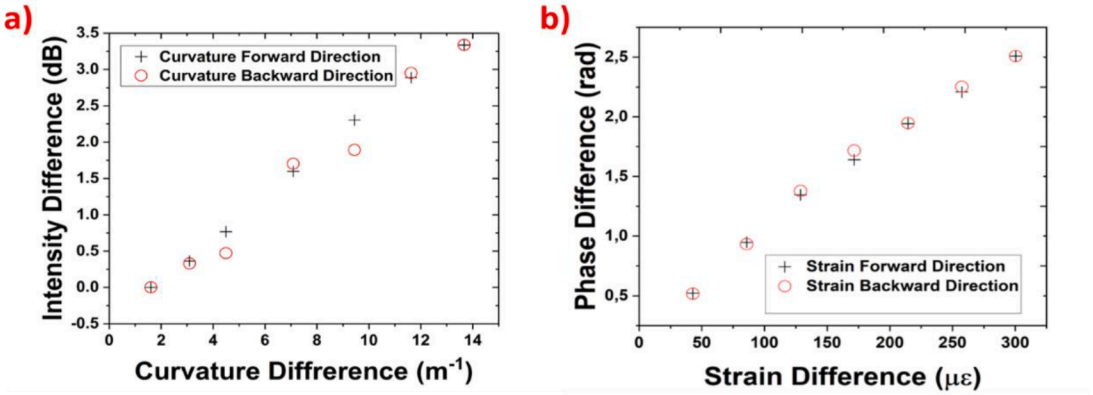

Fig. 14. a) Curvature and b) strain hysteresis analysis, using differential phase (strain) and intensity (curvature).

transform of the spectrum is shown in Fig. 6b. The modulation frequency spectrum indicates that the high order mode, centered at 1.27 nm^{-1}, decreases as the curvature increases. This mode is highly susceptible to fiber bending because its energy is mostly in the cladding; as the curvature increases, the modal energy is lost and the interference with this mode disappears. The modal decrease presents a linear decrement response as the curvature increases. By considering the 1.6 m^{-1} peak power value as a reference, a power loss of around 3.14 dB when the total curvature is applied, was estimated; then a sensitivity of 0.26 dB/m^{-1} is achieved. The modulation component at 0.33 nm^{-1} remains in place as the other mode almost disappears.

The second probe was fabricated using the parameters mentioned in the fabrication setup. The interference spectrum of the second probe is presented in Fig. 7a. Although this spectrum does not show a clear contribution of the high frequency, its spatial component is clearly observed and can be analyzed. As can be observed in Fig. 7b, the high-frequency component decrease as the curvature increases. At the same time, the frequency component related to the lower frequency remains without linear or significant amplitude changes. The interference and the spatially modulated spectrum of probe 3 (fabricated by the same process) are shown in Fig. 8. This probe shows that the high-frequency component is altered as the curvature is applied, and its amplitude value decreases as the curvature increases; this is the same response as previous probes (see Fig. 8b).

The second parameter to be analyzed is the strain; this parameter is applied over T1. It is well-known that strain provides a phase modulation, and this effect can be observed in Fig. 9a (first probe). Furthermore, the wavelength shift direction is towards shorter wavelengths. The

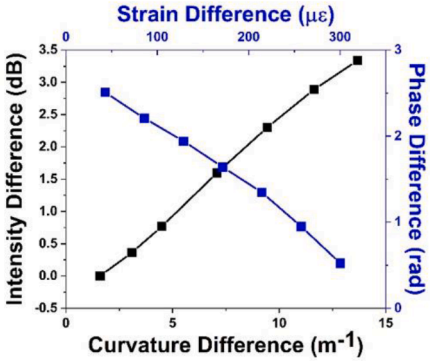

Fig. 15. Simultaneous detection of curvature and strain using phase and intensity demodulation process via Fourier spectrum.

Table 2
Comparative table in terms of range sensitivity and parameters considering prior works.

Parameter	RANGE	Sensitivity	Reference
Strain	0–1939.2 με	0.12 pm/με	[32]
Strain	0–2000 με	1.19 pm/με	[33]
Strain	0–2000 με	1.08 pm /με	[34]
Strain	128–429 με	1.20 pm/με	This Work
Curvature	0–5 m^{-1}	−0.152 dB/m1	[35]
Curvature	0–80 m^{-1}	0.11 dB/m1	[36]
Curvature	0–50 m^{-1}	0.0007 a.u./m − 1	[37]
Curvature	3.1–13.6 m^{-1}	0.32 dB/m^{-1}–0.006 $a.u/m^{-1}$	This Work

strain is also analyzed in a specific wavelength range. The application of strain does not affect the amplitude of the modulation component centered at 1.3 nm^{-1} as can be observed in Fig. 9b. The phase modulation presented by the strain effect can be quantified using complex values of the Fourier Transform at the peak frequency of interest. It is important to mention that the wavelength spectrum exhibits a sensitivity around 1.2 pm/με.

The strain analysis was repeated for the second probe (see Fig. 10a); at this point, the strain was also applied on T1. The interference spectrum shows a wavelength shift in the same direction as in the previous probe. It is important to note that the strain affects the shape of the spectrum; as a result, the Fourier spectrum components will be altered. This issue can be verified at the spectral modulation frequencies centered at 0.35 nm^{-1} and 1.45 nm^{-1}. Moreover, it can be observed that the frequency component related to strain is significantly altered for the strain value of 300 με (see Fig. 10b). The challenges mentioned above can be minimized by decreasing the dynamic range and by choosing the spatial frequency component centered at 1.07 nm^{-1} for the curvature analysis. This component does not exbibit power fluctuations as the strain increase. Moreover, this component shows power variations as the curvature is applied (see Fig. 7b).

In the third probe, the strain also generates a wavelength shift (see Fig. 11). However, in the second probe, the spectrum's shape limits the dynamic range. The technique can be applied even at the spectrum shown in Fig. 11a. According to the spectra modulation frequency (see Fig. 11b), the spatial frequency component used in the curvature analysis remains with minimal power variations.

As observed in the Fourier spectrum, both parameters (strain and curvature) are linked to specific spatial frequency components. By proper processing, it is possible to obtain information about the curvature and strain; The phase difference from the lower spatial frequencies provides information about the strain, while the higher spatial frequencies give information related to the curvature. These peaks are generated by specific sections of dual optical fiber taper structure. In Table 1, the peak components used to monitor strain and curvature are shown. The obtained values show that the fabrication process is reproducible. The first component (strain) will show a similar signal period and the corresponding curvature component. It is important to recall that the curvature component was modified to avoid cross measurement in the second probe.

The repeatability was also evaluated; Three rounds were performed for each probe, as shown in Fig. 12 for strain and in Fig. 13 for curvature. The phase information is extracted using complex values of the Fourier transform at the strain frequency peaks. Meanwhile, the curvature information is obtained using the amplitude of the curvature frequency peaks.

The curvature repeatability analyses of probe 1 (Fig. 12a) and probe 3 (Fig. 12c) show very similar response as the curvature increases and show sensitivities of 0.26 dB/m^{-1} and 0.32 dB/m^{-1}, respectively. Although probe 2 has a higher polynomial response, the sensitivity is similar to the one exhibited by probe 3 (0.28 dB/m^{-1}). It is important to remember that different spectral components were chosen to avoid a cross measurement error during the curvature analysis of probe 2.

The phase analysis of the strain shows linear response, and the maximum sensitivity achieved was 8 mrad/με. The other sensitivities are lower (7.5 mrad/με for probe 2 and 4 0.4 mrad/με and probe 3). However, this is related to the limited dynamic range. The analysis where the maximum sensitivity was achieved indicates minimal trajectory variations and a relative error, close to 0.00107 for curvature. The strain analyses indicate a maximum relative error, close to 0.07. Furthermore, the adjusted squared (R2) indicates good linearity with a value close to 0.9908. By considering the first sample the hysteresis analysis was conducted of both parameters is evaluated in Fig. 8. The curvature analysis shows a path difference of 0.06 dB/m^{-1}, for this case the sensitivity is close to 0.26 dB/m^{-1} (see Fig. 8a). The strain hysteresis indicates a minimal path difference of 0.2 rad (see Fig. 8b). Furthermore, a sensitivity around 8 mrad/με is achieved.

Finally, the simultaneous analysis was conducted for the probe with high sensitivity and the response it is presented in Fig. 14. considering the modulation frequency points where this information is extracted it can be said that the system operates as two independent detection systems. It is important to note that at the moment of applying the strain, the peak component used for curvature detection exhibits a nonlinear response; here, a power variation of 0.8 dB can be appreciated. This variation does not compromise the simultaneous detection (Fig. 15).

At this point, both the strain wavelength sensitivity value and the curvature intensity responses can be compared with prior works in Table 2; This table indicates that the results are competitive with prior works.

6. Conclusions

A fiber-taper system and signal processing technique for the simultaneous detection of curvature and strain was experimentally demonstrated. The technique uses a Fourier transform of the interference spectrum; The spectrum is generated by an optical fiber structure based on two concatenated optical fiber tapers; these tapers were fabricated by using a pulling process and a ceramic micro-heater. The first taper T1 has a diameter close to 2 μm and a length of 3.5 cm. The second taper has a length of 800 nm and a diameter of 4.5 cm. According to our simulations, the second taper generates more energy in the cladding. The Fourier spectrum allows to correlate the modulation frequency components to specific physical parts of the concatenated optical fiber structure. As a result, it was possible to influence these components separately while applying curvature and strain. Here, the strain was studied using the lower frequencies components, and the curvature information was analyzed using higher frequencies components. The curvature was applied over an un-tapered region, where the high order modes generated by the second taper where easily removed. Therefore, the modulation frequency component is amplitude modulated. The wavelength shift was correlated to phase values that correspond to the

complex values of the Fourier spectrum. Three samples were fabricated to probe the repeatability, and the strain and curvature analyses were conducted. The Fourier spectrum shows similar frequency components, which means that the signals have similar periods. As a result, it can be concluded that these optical fiber structures are reproducible. Furthermore, the curvature sensitivity was very similar: 0.26 dB/m^{-1} (Probe 1), 0.32 dB/m^{-1} (Probe 2) and 0.28 dB/m^{-1} (Probe 3). The response fits an exponential model with a standard error close to 0.00107. In addition, hysteresis shows a minimal path variation of 0.06 dB/m^{-1}. The strain sensitivities using the phase analysis were: 8 mrad/με (Probe1), 7.5 mrad/με (Probe 2) and 4.4 mrad/με (Probe 2). Furthermore, the hysteresis analysis of probe 1 showed minimal hysteresis path variation (0.2 rad) and linear response with an adjusted R square of 0.9908. The system and the technique offer the possibility to detect simultaneously curvature and strain. Furthermore, the technique allows to detect minimal variations that cannot be easily detected using traditional techniques.

Declaration of Competing Interest

The authors declare that they have no known competing financial interests or personal relationships that could have appeared to influence the work reported in this paper.

Acknowledgements

J.R. Ek-Ek is grateful to IPN-CIITEC and CONACYT in Mexico for the support under the scholarship 744337, and the Optical Sciences group at The University of Twente in The Netherlands for financing their projects. D. Jauregui-Vazquez appreciates the support of the Optical Sciences Group at the University of Twente and CONACYT Sabbatical Stay 2021 290595.

References

[1] P. Dumais, A. Villeneuve, P.G.J. Wigley, F. Gonthier, S. Lacroix, G.I. Stegeman, J. Bures, Enhanced self-phase modulation in tapered fibers, Opt. Lett. 18 (23) (1993) 1996, https://doi.org/10.1364/OL.18.001996.

[2] H. Li, L. Wei, X. Zhang, Y. Song, Supercontinuum generation in tapered fibers, Opt. InfoBase Conf. Pap. 25 (19) (2009) 1415–1417, https://doi.org/10.1364/acp.2009.wl14.

[3] Y. Jung, Y. Jeong, G. Brambilla, D. J. Richardson, Selective excitation of the fundamental mode in a multimode fiber using an adiabatically tapered splice, in: 2009 14th Optoelectron. Commun. Conf. OECC 2009, vol. 34, no. 15, pp. 2369–2371, 2009, doi: 10.1109/OECC.2009.5213229.

[4] A.B. Taher, P. Di Bin, F. Bahloul, E. Tartaret-Josnière, M. Jossent, S. Février, R. Attia, Adiabatically tapered microstructured mode converter for selective excitation of the fundamental mode in a few mode fiber, Opt. Express 24 (2) (2016) 1376, https://doi.org/10.1364/OE.24.001376.

[5] S. Korposh, S.W. James, S.W. Lee, R.P. Tatam, Tapered Optical Fibre Sensors: Current Trends and Future Perspectives, Sensors (Basel), 19(10) (2019). doi: 10.3390/s19102294.

[6] K.Q. Kieu, M. Mansuripur, Biconical fiber taper sensors, IEEE Photonics Technol. Lett. 18 (21) (2006) 2239–2241, https://doi.org/10.1109/LPT.2006.884742.

[7] H. Latifi, M.I. Zibaii, S.M. Hosseini, P. Jorge, Nonadiabatic tapered optical fiber for biosensor applications, Photon. Sensors 2 (4) (2012) 340–356, https://doi.org/10.1007/s13320-012-0086-z.

[8] H. Xin, R. Xu, B. Li, Optical trapping, driving, and arrangement of particles using a tapered fibre probe, Sci. Rep. 2 (1) (2012), https://doi.org/10.1038/srep00818.

[9] Y. Lou, D. Wu, Y. Pang, Optical Trapping and Manipulation Using Optical Fibers, Adv. Fiber Mater. 1 (2) (2019) 83–100, https://doi.org/10.1007/s42765-019-00009-8.

[10] M.I. Md Ali, S.A. Ibrahim, M.H. Abu Bakar, A.S.M. Noor, S.B. Ahmad Anas, A. K. Zamzuri, M.A. Mahdi, Tapered-EDF-Based Mach-Zehnder Interferometer for Dual-Wavelength Fiber Laser, IEEE Photonics J. 6 (5) (2014) 1–9, https://doi.org/10.1109/JPHOT.2014.2361642.

[11] A.W. Al-Alimi, M.H. Abu Bakar, N.H. Zainol Abidin, A.F. Abas, M.T. Alresheedi, M. A. Mahdi, Dual-wavelength thulium-doped fiber laser assisted by non-adiabatic tapered fiber, Opt. Laser Technol. 112(August 2018) (2019) 26–29. doi: 10.1016/j.optlastec.2018.10.038.

[12] Z. Huang, X. Lei, Y.e. Liu, Z. Wang, X. Wang, Z. Wang, Q. Mao, G. Meng, Tapered Optical Fiber Probe Assembled with Plasmonic Nanostructures for Surface-Enhanced Raman Scattering Application, ACS Appl. Mater. Interfaces 7 (31) (2015) 17247–17254, https://doi.org/10.1021/acsami.5b04202.

[13] N. Díaz Herrera, Ó. Esteban, M.C. Navarrete, A. González-Cano, E. Benito-Peña, G. Orellana, Improved performance of SPR sensors by a chemical etching of tapered optical fibers, Opt. Lasers Eng. 49 (8) (2011) 1065–1068, https://doi.org/10.1016/j.optlaseng.2011.03.012.

[14] W. Bin Ji, H.H. Liu, S.C. Tjin, K.K. Chow, A. Lim, Ultrahigh sensitivity refractive index sensor based on optical microfiber, IEEE Photonics Technol. Lett. 24 (20) (2012) 1872–1874, https://doi.org/10.1109/LPT.2012.2217738.

[15] D. Jauregui-Vazquez, J.W. Haus, A.B.H. Negari, J.M. Sierra-Hernandez, K. Hansen, Bitapered fiber sensor: Signal analysis, Sensors Actuators, B Chem. 218 (2015) 105–110, https://doi.org/10.1016/j.snb.2015.04.109.

[16] S. Mas, J. Martí, J. Palací, Curvature investigation in tapered fibers and its application to sensing and mode conversion, Opt. Lasers Eng. 74 (2015) 109–113, https://doi.org/10.1016/j.optlaseng.2015.05.011.

[17] L.A. Herrera-Piad, J.W. Haus, D. Jauregui-Vazquez, Y. Lopez-Dieguez, J. M. Estudillo-Ayala, J.M. Sierra-Hernandez, J.C. Hernandez-Garcia, R. Rojas-Laguna, A dual modality optical fiber sensor, J. Mod. Opt. 65 (3) (2018) 342–347, https://doi.org/10.1080/09500340.2017.1397220.

[18] F.J. Arregui, I.R. Matías, M. López-Amo, Optical fiber strain gauge based on a tapered single-mode fiber, Sensors Actuators, A Phys. 79 (2) (2000) 90–96, https://doi.org/10.1016/S0924-4247(99)00272-1.

[19] J. Wu et al., Magnetic-field sensor based on core-offset tapered optical fiber and magnetic fluid, J. Opt. (United Kingdom) 16(7) (2014). doi: 10.1088/2040-8978/16/7/075705.

[20] C.-L. Lee, W.-C. Shih, J.-M. Hsu, J.-S. Horng, Asymmetrical dual tapered fiber Mach-Zehnder interferometer for fiber-optic directional tilt sensor, Opt. Express 22 (20) (2014) 24646, https://doi.org/10.1364/oe.22.024646.

[21] L.-Y. Shao, J. Albert, Compact fiber-optic vector inclinometer, Opt. Lett. 35 (7) (2010) 1034, https://doi.org/10.1364/ol.35.001034.

[22] A. Layeghi, H. Latifi, O. Frazao, Magnetic field sensor based on nonadiabatic tapered optical fiber with magnetic fluid, IEEE Photonics Technol. Lett. 26 (19) (2014) 1904–1907, https://doi.org/10.1109/LPT.2014.2341662.

[23] S. Choi, S.-L. Lee, J. Kim, M.S. Kim, D.K. Kim, Y.W. Lee, Tapered Length Dependence of Pressure Sensitivity in Polarimetric Fiber Pressure Sensor Based on Tapered High Birefringence Fiber, IEEE Sens. J. 20 (5) (2020) 2492–2503, https://doi.org/10.1109/JSEN.736110.1109/JSEN.2019.2952925.

[24] P. Lu, L. Men, K. Sooley, Q. Chen, Tapered fiber Mach-Zehnder interferometer for simultaneous measurement of refractive index and temperature, Appl. Phys. Lett. 94 (13) (2009) 94–97, https://doi.org/10.1063/1.3115029.

[25] Z. Wang, G. Zhu, Y.u. Wang, M. Li, R. Singh, B. Zhang, S. Kumar, Fabrication techniques and stability analysis of SMF-/MMF-based differently tapered optical fiber structures, Appl. Opt. 60 (7) (2021) 2077, https://doi.org/10.1364/AO.418875.

[26] G. Zhu, N. Agrawal, R. Singh, S. Kumar, B. Zhang, C. Saha, C. Kumar, A novel periodically tapered structure-based gold nanoparticles and graphene oxide – Immobilized optical fiber sensor to detect ascorbic acid, Opt. Laser Technol. 127 (2020) 106156, https://doi.org/10.1016/j.optlastec.2020.106156.

[27] P. G, R. Jha, Artificial Receptor-Based Optical Sensors (AROS): Ultra-Sensitive Detection of Urea, Adv. Photonics Res. 2(2100044) (2021).

[28] P. Lu, J. Harris, Y. Xu, Y. Lu, L. Chen, X. Bao, Simultaneous refractive index and temperature measurements using a tapered bend-resistant fiber interferometer, Opt. Lett. 37 (22) (2012) 4567, https://doi.org/10.1364/ol.37.004567.

[29] A.G. Leal-Junior, A. Theodosiou, C.R. Diaz, C. Marques, M.J. Pontes, K. Kalli, A. Frizera, Simultaneous measurement of axial strain, bending and torsion with a single fiber bragg grating in CYTOP fiber, J. Light. Technol. 37 (3) (2019) 971–980, https://doi.org/10.1109/JLT.5010.1109/JLT.2018.2884538.

[30] O. NTT Technologies, ceramic micro heaters, vol. id. Copyright 2019 by AMS Technologies Rev. 58-20-01 Ceramic micro heaters info@amstechnologies.com, pp. 1–4, 2019.

[31] J.R. Ek-Ek, F. Martinez-Pinon, J.A. Alvarez-Chavez, D.E. Ceballos-Herrera, R. Sanchez-Lara, H.L. Offerhaus, Fundamental mode intensity evolution in tapered optical fibres, Laser Phys. 30 (12) (2020) 126204, https://doi.org/10.1088/1555-6611/abbe1e.

[32] H. Sun, S. Yang, X. Zhang, L. Yuan, Z. Yang, M. Hu, Simultaneous measurement of temperature and strain or temperature and curvature based on an optical fiber Mach-Zehnder interferometer, Opt. Commun. 340 (2015) 39–43, https://doi.org/10.1016/j.optcom.2014.11.085.

[33] C. Li, T. Ning, X. Wen, J. Li, J. Zheng, H. You, H. Chen, C. Zhang, W. Jian, Strain and temperature discrimination using a fiber Bragg grating and multimode interference effects, Opt. Commun. 343 (2015) 6–9, https://doi.org/10.1016/j.optcom.2014.12.066.

[34] L. Htein, D.S. Gunawardena, C.Y. Leong, H.-Y. Tam, Bragg Gratings in Two-Core Rectangular Fiber for Discrimination of Curvature, Strain, and Temperature Measurements, IEEE Trans. Instrum. Meas. 70 (2021) 1–7, https://doi.org/10.1109/TIM.1910.1109/TIM.2020.3035528.

[35] S. Novais, S.O. Silva, O. Frazão, Curvature detection in a medical needle using a Fabry-Perot cavity as an intensity sensor, Meas. J. Int. Meas. Confed. 151 (2020) 107160, https://doi.org/10.1016/j.measurement.2019.107160.

[36] W. Cui, J. Si, T. Chen, X. Hou, Compact bending sensor based on a fiber Bragg grating in an abrupt biconical taper, Opt. Express 23 (9) (2015) 11031, https://doi.org/10.1364/oe.23.011031.

[37] Y. Wei, J. Hu, C. Liu, B.o. Li, P. Wu, Y. Su, X. Zhao, L. Li, Z. Zhang, M. Cai, Fiber semi-film SPR curvature sensor with the function of directional recognition, Results Opt. 1 (2020) 100003, https://doi.org/10.1016/j.rio.2020.100003.